Impact of shape-optimization on the unsteady aerodynamics and performance of a centrifugal turbine for ORC applications

Giacomo Persico*, Alessandro Romei, Vincenzo Dossena, Paolo Gaetani

Laboratorio di Fluidodinamica delle Macchine, Dipartimento di Energia, Politecnico di Milano, Via Lambruschini 4, Milano, 20156, Italy

This paper presents the results of the application of a shape-optimization technique to the design of the stator and the rotor of a centrifugal turbine conceived for Organic Rankine Cycle (ORC) applications. Centrifugal turbines have the potential to compete with axial or radial-inflow turbines in a relevant range of applications, and are now receiving scientific as well as industrial recognition. However, the non-conventional character of the centrifugal turbine layout, combined with the typical effects induced by the use of organic fluids, leads to challenging design difficulties. For this reason, the design of optimal blades for centrifugal ORC turbines demands the application of high-fidelity computational tools. In this work, the optimal aerodynamic design is achieved by applying a non-intrusive, gradient-free, CFD-based method implemented in the in-house software FORMA (Fluid-dynamic OptimizeR for turboMachinery Aerofoils), specifically developed for the shape optimization of turbomachinery profiles. FORMA was applied to optimize the shape of the stator and the rotor of a transonic centrifugal turbine stage, which exhibits a significant radial effect, high aerodynamic loading, and severe non-ideal gas effects. The optimization of the single blade rows allows improving considerably the stage performance, with respect to a baseline geometric configuration constructed with classical aerodynamic methods. Furthermore, time-resolved simulations of the coupled stator-rotor configuration shows that the optimization allows to reduce considerably the unsteady stator-rotor interaction and, thus, the aerodynamic forcing acting on the blades.

Keywords:
Centrifugal turbine ORC
power systems Shape-
optimization
Evolutionary algorithm
Stator-rotor interaction
Aerodynamic forcing

1. Introduction

Among the several industrial application of organic fluids, Organic Rankine Cycle (ORC) power systems represent one of the most attractive technology for the exploitation of energy sources featuring medium-low enthalpy level [1]. As well known ([2] [3]), the performance of the whole ORC power system is crucially determined by the efficiency of the turbine, whose optimization is complicated by the character of organic fluids, which combine low enthalpy drops with high expansion ratios. The low enthalpy drop has historically led to compact configurations with relatively low number of stages, featuring supersonic flows, converging-diverging cascades and strong shocks at blade outlet regions [4,5]. The subsequent limitations in the design and (especially) off-design turbine performance call for layouts featuring higher number of stages in present-day ORC turbines, accepting an increased size of the machine.

With the aim of preserving compactness while increasing the number of stages, the novel radial-outflow or centrifugal turbine represents a valid alternative to conventional layouts, and it is now receiving scientific [6] as well as industrial [7] recognition. The centrifugal layout allows disposing many stages in a relatively compact device, reducing the cascade expansion ratios and, hence, avoiding supersonic flow conditions. Furthermore, centrifugal turbines can properly accomplish the large volumetric flow ratio thanks to the inherent increase of passage area along the flow path, thus limiting the flaring angle without significant increase in meridional flow component. For these reasons, this set-up has the potential for achieving high aerodynamic performance as well as wide power control capability.

A research program on the development of novel centrifugal turbines for ORC applications is presently ongoing at Politecnico di Milano, with the aim of identifying specific design guidelines for this technology. To this end, a design methodology has been conceived with a hierarchical approach, first considering the

* Corresponding author.
E-*mail address:* giacomo.persico@polimi.it (G. Persico).

Published Journal Article available at: https://doi.org/10.1016/j.energy.2018.09.044

preliminary design on the basis of mean-line and throughflow codes [6], then laying-down basic criteria for the aerodynamic design of centrifugal turbine profiles [8], and finally focusing on the three-dimensional aerodynamics of centrifugal turbine blade rows [9].

As a step forward of this study, the optimal design of a centrifugal turbine stage (considering both the stator and the rotor blades) is proposed in the present paper. Due to the non conventional configuration, the identification of the optimal shapes for centrif-ugal turbine blades working with organic fluids demands the application of an automated and systematic technique based on high-fidelity computational tools and optimization strategies. The procedure here applied is constructed by combining a geometrical parametrization technique, a Computational Fluid Dynamic (CFD) model, and a surrogate-based gradient-free optimization method. High-fidelity steady and time-resolved calculations of the flow in the stage are then performed for both the baseline and optimal configurations, to investigate the effects of optimization on both the stage efficiency and the unsteady aerodynamics of stator and rotor blades.

This paper is structured as follows. At first the stage configuration and the construction of the baseline configuration for the turbine blades are recalled. Then the shape optimization of the two blades is presented. Finally the unsteady flow in turbine stage and the stage performance are presented and discussed.

2. Baseline blade configuration

The centrifugal blade rows studied in this work were conceived for application in the six-stage ORC centrifugal turbine proposed in Ref. [6] operating with MDM as working fluid. Operating conditions, size, power release, and aerodynamic efficiency resulting from the preliminary design were discussed in Ref. [6] and are recalled here in Table 1.

The layout of the turbine consists in six 0.5 reaction stages, each of them featuring the same discharge flow angle (66.7 deg, opposite in sign between stators and rotors), and the same blade meridional chord (26 mm). The six-stage arrangement allows limiting the flow regime to transonic conditions, despite the large pressure ratio. The throughflow analysis, performed with the in-house code TzFlow [10] and reported in Fig. 1, highlights the smooth shape of the meridional channel. The axisymmetric distribution of Mach num-ber (relative on the left frame and absolute on the right frame of Fig. 1) confirms that the flow is transonic or weakly supersonic.

The present work discusses the aerodynamic implications of applying a shape-optimization technique to the centrifugal nozzle and to the centrifugal rotor of the first stage of the turbine, referred to as CN-I and CR-I in the following. The first stage of the machine has an overall total-static expansion ratio of 2; both the rotor and the stator cascades are transonic but their outlet Mach number does not exceed unity, hence converging blade channels were considered. In present-day turbomachinery design, simple criteria are first applied to identify a preliminary shape configuration, which is then optimized using an automatic technique. In the present study, the preliminary (or baseline) shape of the two blade profiles were obtained by applying the technique proposed in Ref. [8], which suggests to adopt profiles featuring an elliptic-arc mean line to induce a sufficiently smooth acceleration of the flow along the blade channel. Then, a conventional distribution of thickness was applied to the mean-line to construct the blade. The resulting profiles, originally constructed in the Cartesian coordinate system, were finally mapped on the polar one using a conformal transformation, in order to maintain the geometric angles of the blade.

Table 1
6-stage turbine conditions, size and performance.

Fluid	$P_{T,in}$	$T_{T,in}$	P_{out}	Ω	D_{out}	*Power*	η_{TT}
MDM	10 bar	274 C	0.17 bar	3000 rpm	1.0 m	1.27 MW	0.869

Fig. 2 reports the layout of the two blade rows under consideration, obtained by applying the aforementioned procedure. The CN-I blade was constructed in order to deflect the flow from radial-outward flow to 66.7 deg; the blade number, selected using the Zweifel criterion, resulted equal to 27. The distribution of thickness was taken from that of a lightly loaded low-pressure axial turbine. The CR-I blade was constructed to deflect the (relative) flow from about +50 deg to −66.7 deg; for such a high aerodynamic loading, the application of the Zweifel criterion led to 52 blades. Moreover, the slender profile shape used for the stator was found to be unsuitable for a blade with turning larger than 90 deg, as flow-detachment might occur in the central part of the profile. For this reason an alternative thickness distribution was assigned, taken from that of a high-pressure turbine blade, resulting in a more advantageous configuration also from the structural point of view.

3. Blade optimization

The progress in computational capability, the increased fidelity of CFD models, and the improved effectiveness of optimization algorithms have recently triggered the development of novel design tools to determine the optimal shape of turbomachinery blades. Among the techniques presently available, deterministic adjoint-based methods [11,12] and heuristic evolutionary methods [13] are nowadays object of intense application and research in Aerodynamics. Evolutionary methods, in particular, are of interest as they allow to explore a wide range of feasible solutions without being 'intrusive' with respect to the source flow model, as they only require the use of direct calculation tools.

In this work, the shape-optimization of the centrifugal blades is carried out by applying the in-house package FORMA (Fluid-dynamic OptimizeR for turbo-Machinery Aerofoils) recently developed at Politecnico di Milano. The optimization strategy, introduced in the following, is constructed by combining three main bricks, i.e. a geometry-parameterization code, a high-fidelity and validated CFD solver, and a surrogate-based evolutionary algorithm.

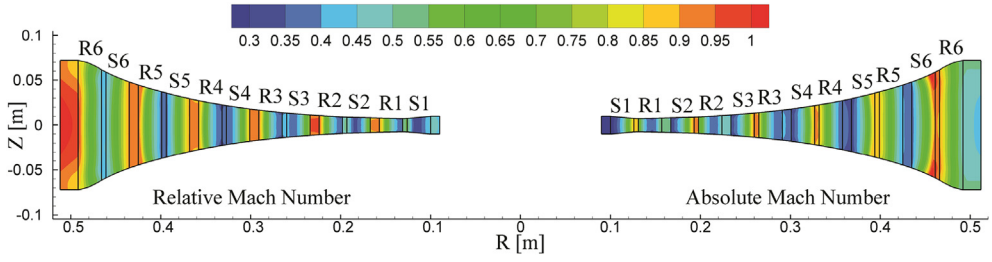

Fig. 1. Distribution of absolute and relative Mach number along the 6-stage centrifugal turbine machine, as resulting from the throughflow calculation.

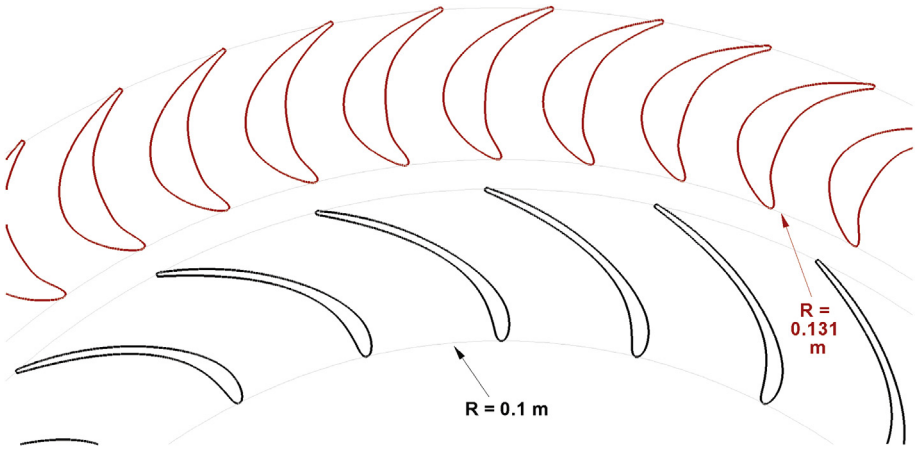

Fig. 2. Baseline configuration of the CN-I (in black, bottom) and the CR-I (in red, top) blade rows assembled in the first stage of the centrifugal turbine.

3.1. Geometry parameterization method

In shape optimization problems, it is common practice to parametrize the geometry with piecewise functions, so to control the shape by moving a limited number of so-called Control Points (CPs). In the FORMA package, B-Spline curves are used to parameterize the blade profile; the global and local control of the shape provided by the use of B-Splines makes them a powerful tool for aerodynamic design [14]. The position of the CPs and their range of variation define the design space of the optimization problem. Piecewise lines of order 3 are used in this work. More details on the parametrization technique can be found in Ref. [15].

To set-up the optimization, at first an approximate representation of the baseline blade shape is constructed using a B-Spline curve, defined and manipulated by the position of the CPs; once the number and the spacing of the CPs is prescribed, the coordinates of the CPs are found via a least squares interpolation method. The pressure and suction sides of the blade are generated as a unique B-Spline curve, filleted by a circular-arc trailing edge.

3.2. Computational flow model

To evaluate the fitness of the configurations progressively selected by the optimization algorithm, CFD simulations are performed using the ANSYS-CFX solver. As only blade-to-blade effects are of interest in this investigation, quasi-3D simulations are carried out, stacking spanwise the same profile generated with the geometry parameterization algorithm, and considering a straight stream-tube around midspan. Turbulence effects are introduced using the $k-\omega$ *SST* model, prescribing wall y^+ below unity all along the blade profile. To introduce the non-ideal thermodynamic behavior of the MDM, a look-up table approach is used. The look-up table was constructed by sampling the Span-Wagner Equations of State [16] though the thermodynamic library *FluidProp* and including tabulated transport properties. A TVD high-resolution numerical scheme [17] is used to discretize the advection terms of the flow and turbulence equations, while second-order central differences are used for the diffusive fluxes.

Calculations are performed on structured grids composed by hexahedral elements; the mesh is re-generated for each CFD run performed throughout the optimization process, so to guarantee that the mesh quality is consistent among all the simulations. To identify the size of the meshes used within the optimization and for the assessment study, dedicated grid sensitivity analyses were performed for both the stator and the rotor. The results of these analyses, fully consistent with those presented in Ref. [8], showed that meshes composed by 100 kcells in the blade-to-blade surface are sufficient for obtaining a grid-independent solution. Moreover, meshes composed by 50 kcells in the blade-to-blade surface were found to provide an optimal trade-off between computational cost (10 min for a CFD run on a 16-processor Linux cluster) and accuracy (overestimates of entropy production below 5% of the grid-independent value). Therefore, these latter were used for the CFD runs within the optimization processes, while grid-independent meshes were used for the assessment calculations performed on the baseline and optimal cascades.

The baseline and optimal configurations were finally assessed after the optimization by means of time-resolved CFD simulations performed with grid independent meshes and using second order accuracy for the discretization of the unsteady term. The reliability of the time-resolved flow model had been previously assessed against unsteady measurements performed by the authors themselves [18]. The CFD model was shown to accurately predict the fully three-dimensional and unsteady flow physics, and provided estimates of stage efficiency within 1% of the experimental datum, i.e. comparable to the uncertainty of the measurement technique.

3.3. Surrogate-based optimization strategy

The optimization techniques implemented in FORMA, and in particular the one applied in this work, are evolutionary strategies (Genetic Algorithms, in particular) combined with surrogate models. Genetic Algorithms (GAs) are attractive as they allow to deal with oscillating and non-smooth objective functions, as well as to easily handle constrained and multi-objective optimization problems [19]. Furthermore, GAs are global optimization methods and, hence, are best suited in presence of a multiplicity of local optima (a situation that cannot be easily excluded *a priori* in aerodynamic design).

Nevertheless, GAs require a massive application of the direct computational tool, that in case of CFD often result in an unacceptable computational burden. To tackle this cost, a surrogate evolutionary strategy was applied in this study. This technique is conceived so that the GA operates only on a surrogate model of the objective function. To be effective, the surrogate model has to be a reliable representation of the objective function; in surrogate-based strategies the model is initialized and progressively updated during the optimization, so that the shape is optimized while the reliability of the surrogate improves. In this work, the objective function is approximated by applying the Kriging meta-model, as it

allows to properly capture the complexity of response surfaces featuring sharp curvature changes, even in presence of highly irregular distributions of interpolation points. This makes the Kriging model suitable for complex optimization problems such as the design of transonic turbomachinery.

In surrogate-based optimization, the model is initialized by interpolating a database of configurations tested with CFD. To improve the reliability of the surrogate model, both Surrogate-Based Local and Global Optimization (SBLO, SBGO) have been developed, the former based on the 'trust region approach' and the latter based on the 'training' concept. In this work, the global method has been applied, as in previous optimization studies of ORC turbine blades it proved to be reliable and computationally efficient [15,20]. In SBGO, the model is 'trained' by progressively adding the optima found during the optimization, and tested with CFD, to the initial database. In this way, the SBGO results compu-tationally efficient; even though the convergence is not strictly guaranteed, previous applications of FORMA [15,20] as well as preliminary trials made at the early stages of this work did not exhibit convergence issues, if a sufficiently large initial data-base is assigned. In particular, the initializations in this study were per-formed by applying a Latin Hypercube technique with a population equal to 10 times the number of design variables.

The surrogate strategies implemented in FORMA package were constructed within the object-oriented framework Dakota [21], that makes available several classes of algorithms and routines for interpolation, optimization, and uncertainty quantification.

3.4. Optimization results

In this work the FORMA package was applied to optimize singularly the blades of the CN-I and the CR-I cascades. The performance of the resulting stage was then evaluated afterwards, by combining the two optimal cascades. The CN-I case is first considered, then the CR-I case is presented.

3.4.1. Centrifugal stator optimization

Despite the moderate level of cascade aerodynamic loading, the design of CN-I is complicated by the significant radial effect. The application of the design method proposed in Ref. [8] to CN-I leads to blades featuring a long and curved region of un-guided turning on the rear suction side. This makes critical the blade aerodynamics, especially considering the transonic flow regime, which may lead to the onset of shocks in the rear part of the profile (see Ref. [9]).

To proper control the CN-I blade aerodynamics, the shape optimization was focused on the rear part of the profile. However, as discussed in detail in Ref. [20], also the front suction side is critical, as adverse pressure gradients might establish in this area. For these reasons, the CN-I baseline geometry was parametrized with 21 CPs, 14 of those are movable by $\pm 0.4mm$ along the direction normal to the local blade surface, as reported in Fig. 3(a). The 4 CPs closest to the trailing edge were kept fixed, so to guarantee the regularity of the blade shape in the region where the B-spline merges with the circular arc; this also allows to constraint the trailing edge thickness and wedge angle.

The objective function was defined as the entropy generation across the cascade in nominal operating condition (i.e., the one resulting from the mean-line optimization).

Fig. 3(b) reports the result of the optimization by comparing the baseline and the optimal blade shapes. The optimization enlarges the blade in the leading edge region, it increases the blade curvature in the central region, and finally it reduces the curvature in the rear region downstream of the throat (thus limiting the un-guided turning). Dedicated high-resolution simulations were performed after the optimization to analyze the results. Fig. 4 reports the Mach number distributions around the baseline and the optimal cascades, and shows that the optimal shape allows to minimize the

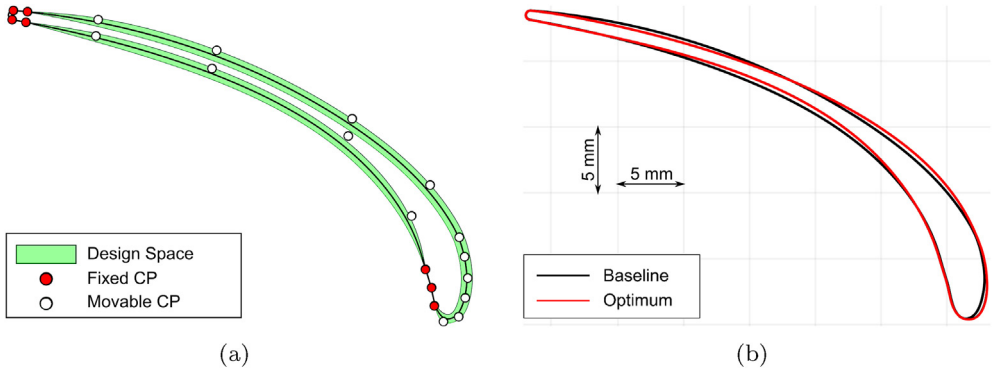

Fig. 3. CN-I optimization: (a) design space definition; (b) baseline and optimal shapes.

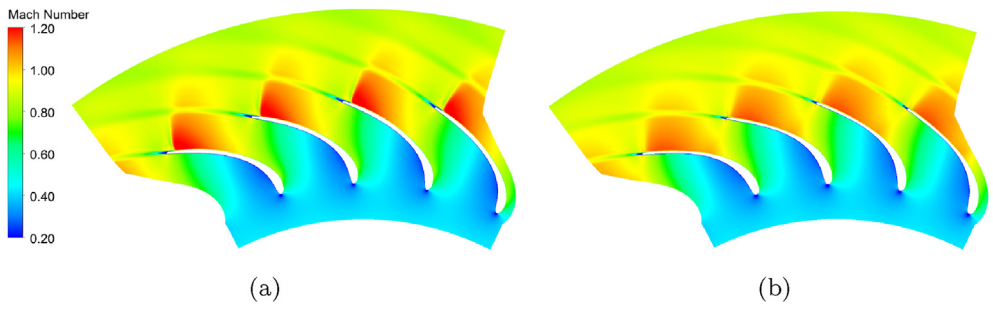

Fig. 4. CN-I aerodynamics: (a) baseline configuration; (b) optimal configuration.

over-speed on the rear suction side. As a result, the shock generated close to the trailing edge is greatly weakened (if not eliminated), with beneficial effects on both the cascade performance and the unsteady aerodynamic forcing acting on the subsequent rotor. The optimization also improves the aerodynamics of the blade in the front part, as testified by the lower gradients in Mach number close the two blade sides, and in general it guarantees a smooth pressure distribution along the whole blade surface. In quantitative terms, the optimization reduces by about 35% the entropy production; to introduce a more explicit quantification of the improvement in cascade performance, the kinetic energy loss coefficient was evaluated, defined as:

$$\zeta_S = \frac{h_{out} - h_{out,is}}{V_{out}^2 / 2} \tag{1}$$

The parameter ζ_S was evaluated half a radial chord downstream of the blade trailing edge, where the flow is almost mixed-out, and it was found to drop from 3.1% to 2% as a result of the stator optimization.

3.4.2. Centrifugal rotor optimization

The optimization of the rotor proved to be much more challenging than the one of the stator. At first, CR-I exhibits very different features with respect to CN-I, but it shares with this latter some design difficulties. The significant curvature in the rear region, required to regularly distribute the very high turning along the whole blade, complicates the design especially on the suction side. The central section of the blade, which features the largest camber and thickness, is also critical, especially for the blade loading control.

These considerations led to parametrize the blade with 20 CPs, assembled as follows: 4 on the leading edge, 7 on the suction side, 5 on the pressure side and 4 on the trailing edge; as highlighted in Fig. 5(a), 10 CPs are movable along the direction normal to the local blade surface by a displacement increasing from $\pm 0.5mm$ in the trailing edge region to $\pm 0.8mm$ in the central part of the blade. Out of these 10 movable CPs, 5 are placed on the suction side, 4 are placed on the pressure side, and one is placed in the trailing edge region. In fact, this latter CP carries back the other three CPs of the trailing edge region, which are moved rigidly with the former. In this way, the blade shape has the proper degree of freedom at the trailing edge while preserving regularity where the B-spline merges with the circular arc; such approach also allows constraining the trailing edge thickness and the wedge angle. Eventually, only the front part of the blade is kept fixed within the optimization process.

The flow model selected to simulate the rotor aerodynamics was based on a previous study of the authors [9], according to that it is mandatory to perform simulations in the rotating frame (i.e., including explicitly the centrifugal and Coriolis contributions into the model) to predict appropriately the flow in centrifugal rotors. The objective function was defined as the entropy generation across the cascade in nominal operating condition (i.e., the one resulting from the mean-line optimization). Preliminary trials indicated that the optimization succeeded in reducing the loss generation, but the optimal configurations were often non-consistent with the stage under consideration, in terms of work exchange and reaction degree. This is motivated by the fact that the flow deflection across rotors determines the work exchange; therefore, individuals producing different flow angles from the design one may alter significantly the operation of the stage and can potentially frustrate the optimization effort.

By virtue of the aforementioned considerations, the rotor optimization was performed introducing a non-linear constraint on the rotor-exit flow angle, which is prescribed to remain within the range 66.5–67 deg. It is to be noted that no constraint was required at the inlet, where the flow angle is imposed as boundary condition. Fig. 5(b) reports the comparison between the baseline and the optimal rotor blade shapes. The optimization alters significantly the central region of the blade, reducing the thickness on both the blade sides. The rear region of the blade is also altered, as the trailing edge is moved azimuthally in such a way to limit the cur-vature in the final part of the blade.

Fig. 6 reports the relative Mach number distributions in the baseline and optimal configurations, as resulting from dedicated rotor stand-alone simulations with a high-resolution mesh. The comparison between the two distributions indicates that the constrained optimization minimizes the over-speed on the rear suction side; this weakens the shock on the rear suction side and attenuates the related boundary layer separation, resulting in a thinner wake shed by the blade. In quantitative terms, the optimization reduces the entropy production by more than 40% while keeping the discharge flow angle equal to its design value (66.7 deg). To quantify the improvement in cascade performance, the kinetic energy loss coefficient was evaluated, defined as:

$$\zeta_R = \frac{h_{out} - h_{out,is}}{W_{out}^2 / 2} \tag{2}$$

The parameter ζ_R was evaluated half a radial chord downstream of the blade trailing edge, where the flow is almost mixed-out, and

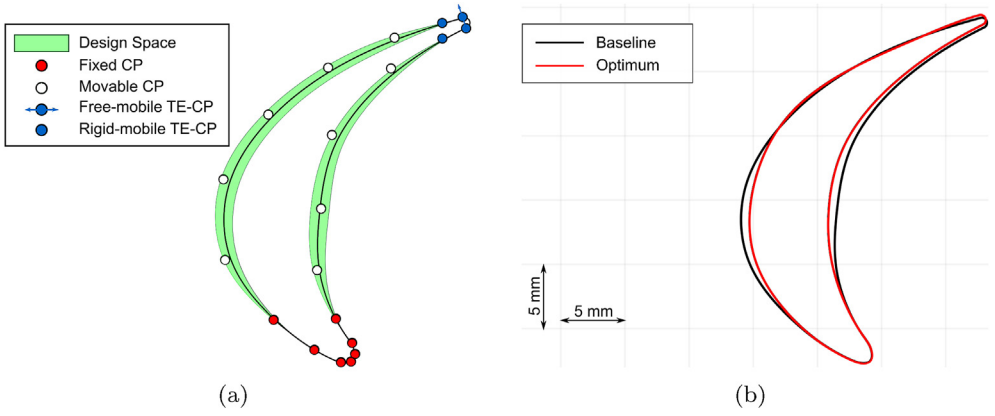

Fig. 5. CR-I optimization. (a): design space definition. (b) baseline and optimal shapes.

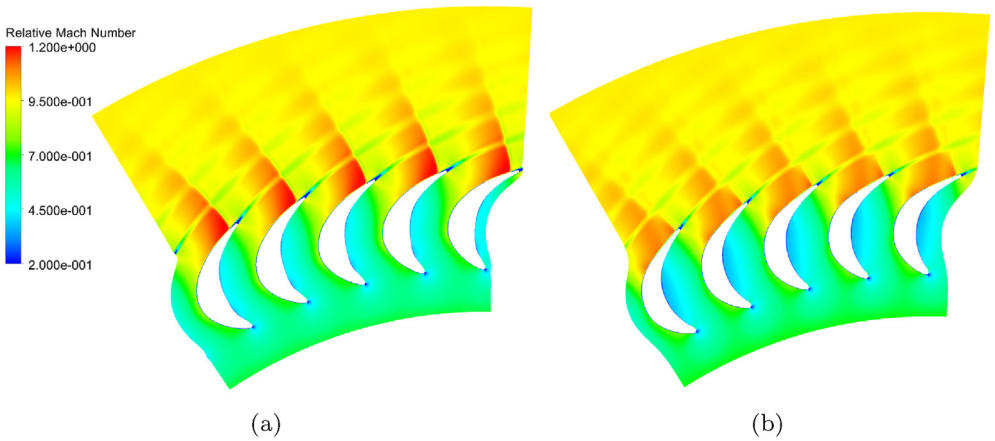

Fig. 6. CR-I aerodynamics: (a) baseline configuration; (b) optimal configuration.

it was found to drop from 4.4% to 2.4% as a result of the optimization.

4. Full stage analysis

The analysis proposed above indicates that the optimization leads to a net reduction of loss generation across both the stator and rotor cascades, once they are studied in stand-alone configuration. To widen the perspective on the impact of optimization, the aero-dynamics and performance of the full stage were investigated by considering unsteady coupled stator-rotor simulations, carried out introducing a sliding mesh between the two cascades. Three stage configurations were considered, namely: (a) the stage featuring the baseline blades (the one shown in Fig. 2); (b) the stage featuring the optimal stator and rotor blades; (c) a hybrid configuration con-structed combining the baseline stator with the optimal rotor. The comparison between cases (a) and (b) directly indicates the quantitative improvement provided by the optimization. The comparison between (b) and (c) cases, that share the rotor blade but feature different stators, allows to highlight the impact of the stator blade optimization on the rotor aerodynamics and on the stator-rotor interaction.

When performing unsteady simulations, a modeling issue arose as the stator and rotor blade numbers (determined by applying the Zweifel criterion, as remarked above) are prime each other (27 vs 52 respectively). As well known, this choice is beneficial for the integral aerodynamic forcing acting on the blade rows, but implies that the actual periodicity is extended to the whole annular cascades, leading to very heavy computational cost if kept unaltered. To tackle this cost, the rotor blade number was increased from 52 to 54 (which is the closest multiple of the stator blade number); in order to keep the shape unaltered, the rotor blade was transformed applying a homothetic scaling, reducing its size by a factor 54/52. Comparative steady-state calculations of the flow in the stage were performed with the original and the scaled rotor and did not show any appreciable difference in terms of flow morphology and stage efficiency. By virtue of the change in rotor blade number, a simplified chorochronic periodicity over one stator pitch and two rotor pitches can be applied, thus dramatically reducing the computational cost of the unsteady calculation. Each unsteady simulation required about 250 h on a 16-processor cluster.

4.1. Stage performance

Considering the potential performance improvement estimated for the single cascades, the stage performance were first analyzed for the cases (a) and (b). The stage performance was defined according to the total-total efficiency definition, which reads:

$$\eta_{TT} = \frac{h_{T,in} - h_{T,out}}{h_{T,in} - h_{out,is} - V_{out}^2/2} \tag{3}$$

The efficiency was evaluated considering a mixed-out flow configuration and on a time-resolved basis. The instantaneous values were then time-averaged to obtain the mean stage performance. For case (a), which features the baseline blades, the time-mean efficiency results 91.9%, with a fluctuation of 1.4% during the blade passing period. For case (b), which features both the optimal blades, the time-mean efficiency results 93.9%, with a fluctuation of 0.75% during the blade passing period. These quan-titative results are interesting for multiple reasons. At first, the relevant quantitative difference between the mean efficiency values demonstrates that the optimization of the single blade rows succeeds in improving the performance of the full stage; this means that the constrained optimization set-up selected for the rotor allows to properly represent (even though implicitly) the coupling between the cascades. On a strictly quantitative ground, the improvement in stage efficiency is sufficiently high for being estimated reliably by the CFD solver; as a matter of fact, comparison against experiments showed that the CFD model here used provides performance estimates within 1% of the experimental value, as reported in Ref. [18].

The analysis of the stage efficiency provides a second relevant indication. Case (b) does not only provides higher performance than case (a), but it also features lower unsteady oscillations in the time-resolved efficiency. Therefore, the stage configuration with baseline blades does experience a higher stator-rotor interaction, that might have an impact also on the aerodynamic forcing on the blades. Unsteady stator-rotor interaction phenomena in centrifugal turbines have never been considered in Literature and, hence, they deserve a specific investigation, which is proposed in the following section.

4.2. Time-resolved stage aerodynamics

The stator-rotor interaction is promoted by the azimuthal gradients that arise upstream and downstream of the blades. The analysis of the stage performance indicates that the use of optimal blades reduces the unsteady oscillation of the flow and, hence, it does also reduce the stator-rotor interaction. To investigate the

impact of the optimization on the stator-rotor interaction, a comparison between cases (b) and (c) is here proposed; cases (b) and (c) couple the optimal rotor blade shape with the optimal and the baseline stator blade respectively. In this way, the effect of the stator shape-optimization can be highlighted, in a context in which the flow around the rotor is not altered by the specific shape of the rotor blade, but only as a consequence of the interaction with the upstream stator.

Fig. 7 reports the instantaneous distributions of absolute Mach number in the whole stage for the case (c) at four instants of the rotor blade passing period (BPP in the following). Such images allow to highlight the shock patterns in-between the blade rows, as well as their impact on the stator aerodynamics in the region of unguided turning and on the rotor aerodynamics in the front section of the blade. As a general consideration, the aerodynamic interaction between the blade rows is very significant, as a result of the transonic nature of the flow and the very small radial gap. In particular, from the beginning ($t/BPP = 0.00$) to the middle ($t/BPP = 0.50$) of the BPP, the flow evolves from a smooth shock-free condition into a configuration featuring a region of super-sonic flow, where the Mach number reaches 1.35, followed by a relatively strong shock impinging on the front section of the rotor blade. The observed evolution of the flow is motivated by the combination between the local expansion regions on the stator and rotor blades. As the rotor sweeps in front of the stator, a diverging 'virtual' duct is generated in-between the rear suction side of the stator and the front suction side of the rotor, promoting the supersonic expansion of the transonic flow discharged by the stator; the shape (in particular, the cross-section variation) of this virtual duct changes with time, altering the instantaneous Mach number distribution in this region. Similar effects were observed in transonic axial gas turbines [22,23]; however, the shape of the virtual duct (and its change with time) is much more difficult to visualize and identify in the present centrifugal layout, as the radial effect makes the cross-section to inherently increase in the stator-rotor gap. In the second part of the period ($t/BPP = 075$) the relative position of stator and rotor determines a virtual duct with a very small divergence, resulting in a lower over-speed and a weakening of the shock.

The frames of Fig. 7 indicate that the non-optimized stator induces large fluctuations on the rotor loading. To highlight the impact of optimization, Fig. 8 reports the same kind of representation of Fig. 7, but for case (b). The flow phenomena and the evolution of the flow are similar to those described for the previous case; nevertheless, the optimization of the stator blade leads to a significant reduction of the over-speed generated in the stator-rotor gap. In the central part of the BPP the supersonic flow re-gion within the virtual duct constituted by the stator and rotor blades still appears, but with a lower maximum Mach number (1.2 against 1.35 of the previous case). Single-cascade simulations show that the optimization reduces the over-speed of the stator blade; this beneficial feature is preserved when the cascade is operated in the actual unsteady condition of the stage, leading to a weaker shock impinging on the rotor and thus reducing the forcing.

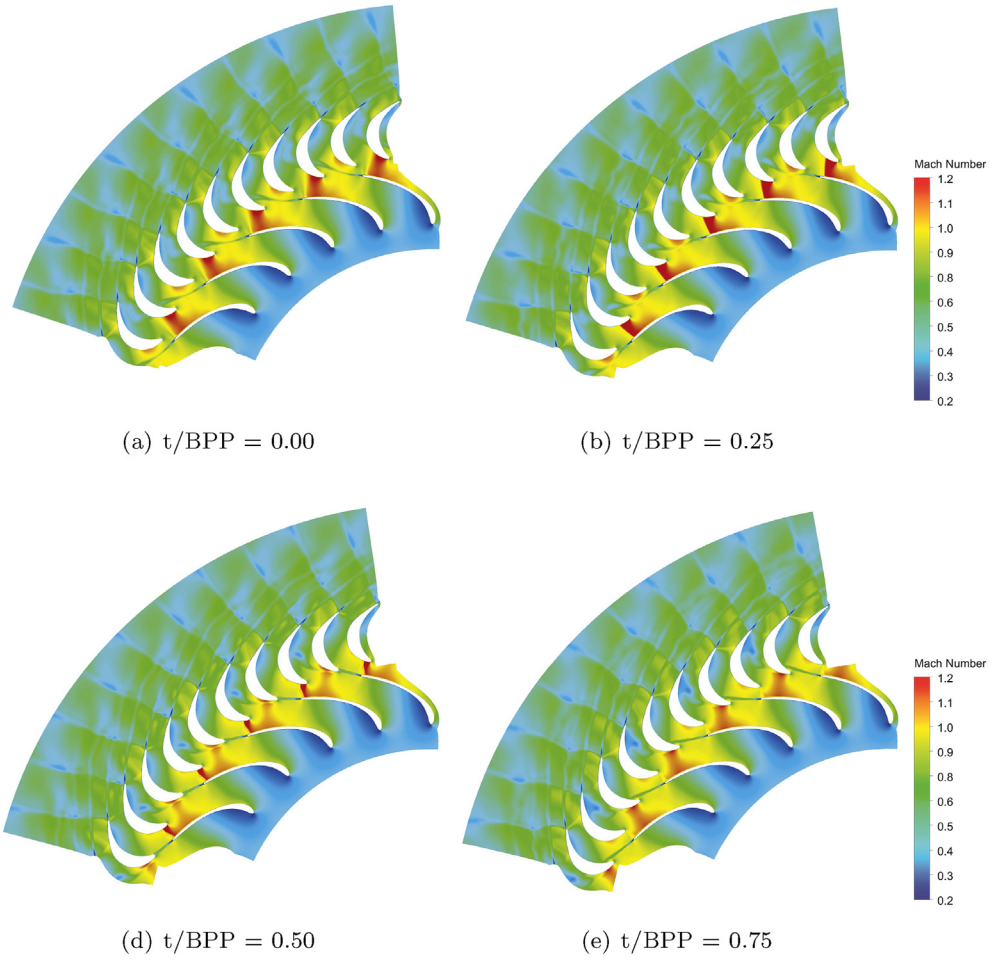

Fig. 7. Case (c): centrifugal turbine stage with baseline stator and the optimal rotor. Instantaneous Mach number distribution.

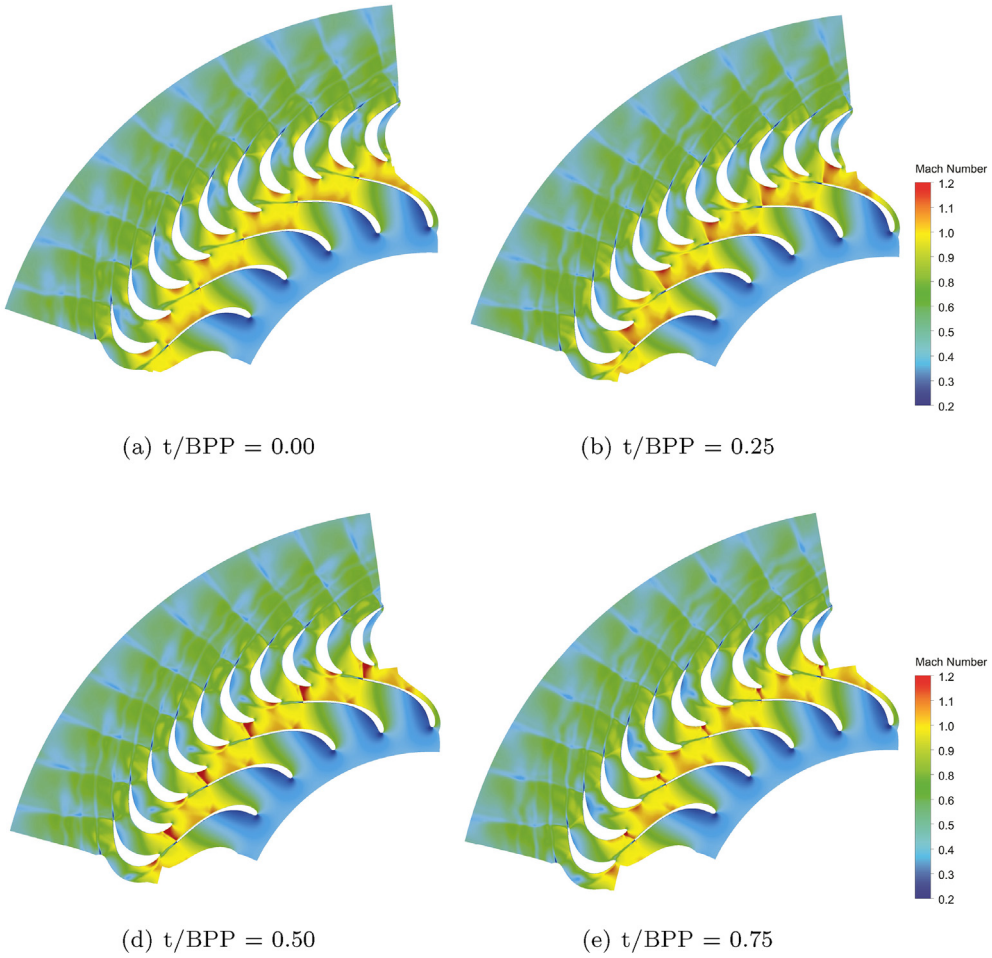

Fig. 8. Case (b): centrifugal turbine stage with optimal stator and rotor blades. Instantaneous Mach number distribution.

To quantify the impact of the optimization on the aerodynamic forcing acting on the rotor, the time-resolved pressure distribution over the rotor blade surface was extracted from the unsteady simulations of cases (b) and (c), and the local pressure fluctuations were determined and compared. Fig. 9 reports, for the two cases, the time-mean pressure distribution on the rotor blade surface, alongside the amplitude of the local pressure fluctuation expressed as Root Mean Square. The comparison shows that adopting the optimal stator reduces significantly the pressure oscillation over the whole rotor blade, especially in its front section. In quantitative terms, the amplitude of the pressure oscillations over the entire blade (and, hence, the aerodynamic forcing acting on the blade) reduces by 17.5%. The highest impact of optimization is found in the front part of the suction side, from the leading edge to the point of maximum camber, where the nozzle shock periodically impinges; in this area, the use of the optimal stator weakens the amplitude of the pressure oscillations by almost 25%.

Alongside stator-rotor interaction effects, the optimization may have an impact also on the interaction between the stages. As already discussed when commenting the CR-I aerodynamics, and as visible from the sharp gradients in absolute Mach number downstream of the turbine, the rotor itself is transonic and generates a relatively strong shock close to the trailing edge. In case (c), the rotor shock is modulated by the interaction between the rotor blade and the wake and pressure field of the stator; in fact, a detailed inspection of the frames of Fig. 7 reveals that flow configuration in the discharge section of CR-I changes significantly during the blade passing period (to have a clear view of the differences, it is sufficient to compare the Mach number distributions on two adjacent rotor channels, that exhibit a phase-lag of half of the period). When looking at the corresponding frames of Fig. 8, related to case (b), the unsteady fluctuation of the rotor shock appears mitigated. As a result, the application of shape-optimization to the stator and the rotor of the stage has a dual effect: the optimization of the CR-I weakens the shock as well as the optimization of the CN-I reduces the shock modulation, potentially minimizing the forcing on the blade rows on the following stage.

Fig. 10 reports the unsteady evolution of the entropy field for the case (b). As the shocks involved are relatively weak, the entropy distribution is dominated by the wakes shed by the cascades; therefore, such representation allows highlighting the process of unsteady wake transport in a centrifugal turbine stage, which is still not documented in Literature. The evolution of wake for case (c) was found to be qualitatively similar to the one of case (b) and it is not reported for sake of brevity. The frames of Fig. 10 show that the wake shed by the nozzle blade are chopped by the rotor blade and then convected downstream towards the suction surface of the rotor blade, taking the typical hairpin shape observed in axial turbines. As a result, at the exit of the stage the stator wakes tend to be accumulated on the suction side of the rotor wakes. The rotor wakes, in turn, exhibit a periodic unsteadiness as a result of the interaction with the flow structures of the stator, which alter periodically the incidence angle and the pressure distribution in the front blade section, thus altering the blade loading and the

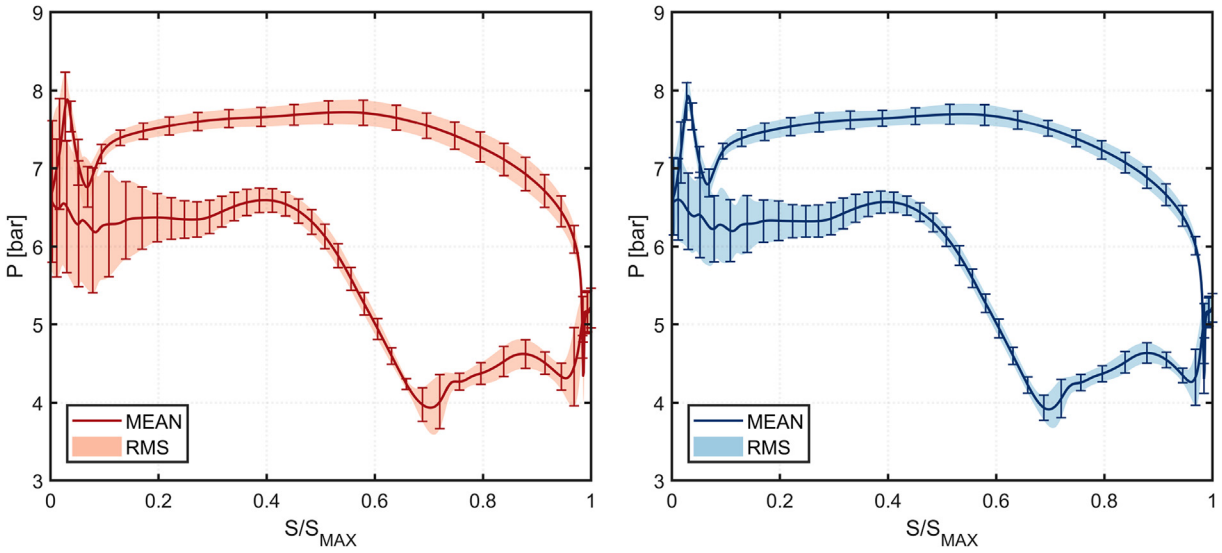

Fig. 9. Mean pressure distribution and RMS of the pressure oscillations on the optimal rotor blade coupled with the baseline (left) and the optimal (right) stator blade. To improve the readability of the diagrams, the RMS is marked both as shaded area and error bar on the time-mean trend.

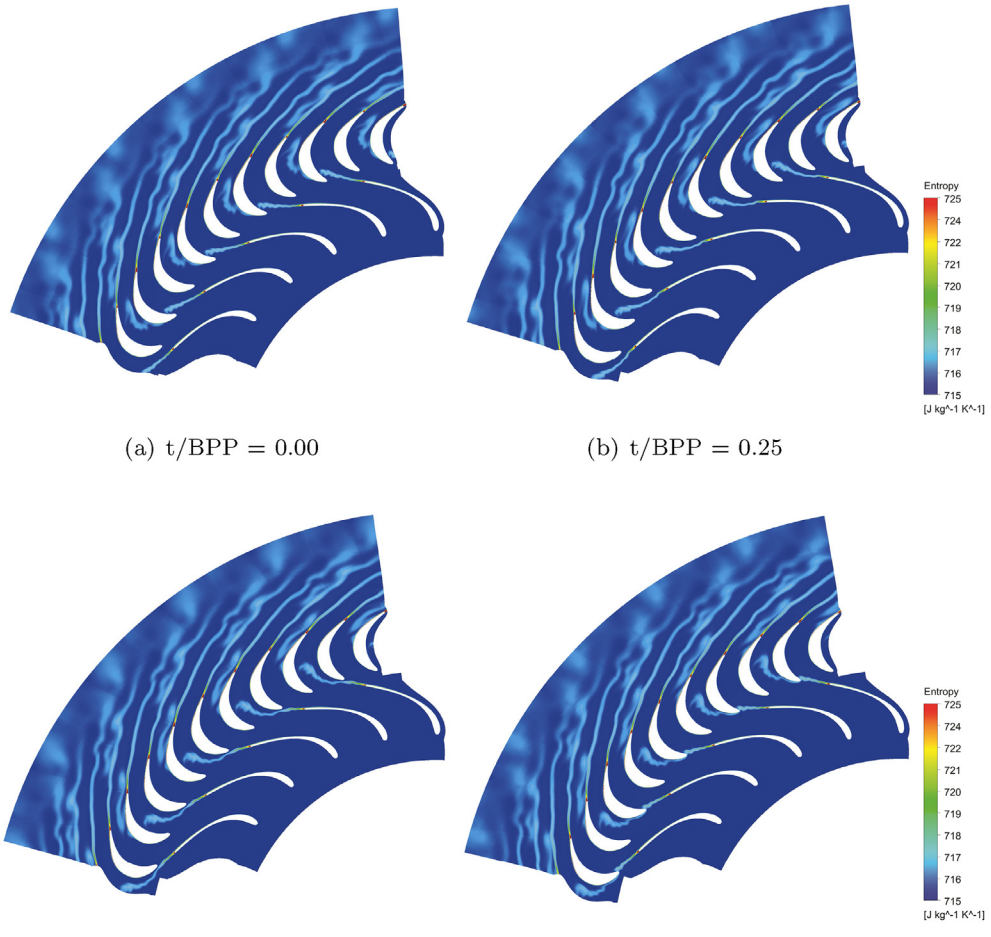

Fig. 10. Case (b): centrifugal turbine stage with optimal stator and rotor blades. Instantaneous entropy distribution.

boundary layer state in the trailing edge region.

5. Conclusions

This paper has presented the application of a shape-optimization technique to the design of a centrifugal turbine stage for ORC application. The technique, implemented in the in-house design package FORMA, makes use of a geometry-parametrization tool, an high-fidelity flow solver, and a surrogate-based evolutionary algorithm.

The baseline shape of the blades, constructed by means of conventional aerodynamic methods, were first parametrized via B-Splines identified by a limited number of control points. An experimentally validated CFD model was used in combination to a look-up table approach for the simulations of non-ideal transonic flow of organic fluids. To tackle the computational cost of the optimization, the evolutionary algorithm was coupled to a Kriging surrogate model.

The results indicate that applying a systematic optimization procedure to a non-conventional turbine configuration leads to several beneficial effects. Overall, the stage efficiency rises by almost 2%, and the stator-rotor interaction is clearly mitigated, thus lowering by 25% the aerodynamic forcing acting on the front part of the rotor blades. A detailed analysis of the optimized configurations indicate that most of the efficiency improvement is achieved by the optimization of the rotor, which has to impart a very high deflection to the flow; conversely, the stator optimization is crucial for reducing the rotor aerodynamic forcing, as the optimal stator minimizes the entropy generation and the azimuthal gradients at the rotor inlet as well.

The investigation presented in this paper has shown that in complex non-conventional configurations, for those well-established design guidelines are still unavailable, a systematic optimization tool like the one here employed can be used not just as a technical instrument for design but also to infer novel design criteria.

Acknowledgments

Authors wish to thank Stefano Zamblera, Viola Papetti, and Valentina Pivetta for their efforts on the preliminary trials and exercises on shape-optimization.

Nomenclature

D	Diameter [m]
BPP	Rotor Blade Passing Period
CFD	Computational Fluid-Dynamics
CP	B-Spline Control Points
CN-I	First Stage Cascade Nozzle
CR-I	First Stage Cascade Rotor
GA	Genetic Algorithm
h	Enthalpy [J/(kg K)]
ORC	Organic Rankine Cycle
P	Pressure [Pa]
T	Temperature [K]
V	Velocity in Stationary Frame [m/s]
W	Velocity in Relative Frame [m/s]

Greek

ζ	Kinetic Energy Loss Coefficient
η_{TT}	Total-to-Total Turbine Stage Efficiency
Ω	Rotational Speed [RPM]

Subscripts

is	Value obtained through isoentropic transformation
in	Inlet of Stage/Cascade
out	Outlet of Stage/Cascade
R	Rotor
S	Stator
T	Total Quantities

References

[1] Gaia M. 30 Years of organic rankine Cycle development. In: First international seminar on ORC power systems, keynote lecture; 2011.

[2] Macchi E. The choice of working fluid: the most important step for a successful organic rankine Cycle (and an efficient turbine). In: Second international seminar on ORC power systems, keynote lecture; 2013.

[3] La Seta A, Meroni A, Andreasen JG, Pierobon L, Persico G, Haglind F. Combined turbine and Cycle optimization for organic rankine Cycle power systemsPart B: application on a case study. Energies 2016;9(393).

[4] Hoffren J,TT, Larjola J, Siikonen T. Numerical simulation of real-gas flow in a supersonic turbine nozzle ring. ASME J Eng Gas Turb Power 2002;124: 395–403.

[5] Harinck J, Colonna P, Guardone A, Rebay S. Influence of thermodynamic models in 2D flow simulations of turboexpanders. ASME J Turbomach 2010;132:011001–17.

[6] Pini M, Persico G, Casati E, Dossena V. Preliminary design of a centrifugal turbine for ORC applications. ASME J Eng Gas Turb Power 2013;135, 042312.

[7] Spadacini C, Centemeri L, Xodo L, Astolfi M, Romano M, Macchi E. A new configuration for Organic Rankine C ycles power systems. In: First international seminar on ORC power systems; 2011.

[8] Persico G, Pini M, Dossena V, Gaetani P. Aerodynamic design and analysis of centrifugal turbine cascades. In: ASME turbo expo 2013. GT2013-95770; 2013.

[9] Persico G, Pini M, Dossena V, Gaetani P. Aerodynamics of centrifugal turbine cascades. ASME J Eng Gas Turb Power 2015;137(112602):1–11.

[10] Persico G, Rebay S. A penalty formulation for the throughflow modeling of turbomachinery. Comput Fluids 2012;60:86–98.

[11] Peter J, Dwight R. Numerical sensitivity analysis for aerodynamic optimization: a survey of approaches. Comput Fluids 2010;39:373.

[12] Pini M, Pasquale D, Persico G, Rebay S. Adjoint method for shape optimization in real-gas flow applications. ASME J Eng Gas Turb Power 2014;137, 032604.

[13] Coello C. An updated survey of GA-based multiobjective optimization techniques. ACM Comput Surv 2000;32(2):109–43. https://doi.org/10.1145/358923.358929.

[14] Farin G. Curves and surfaces for CAGD: a practical guide. fifth ed. San Francisco, CA, USA: Morgan Kaufmann Publishers Inc.; 2002. ISBN 1-55860-737-4.

[15] Rodriguez-Fernandez P, Persico G. Automatic design of ORC turbine profiles using evolutionary algorithms. 3rd international seminar on ORC power systems, vol. 133; 2015.

[16] Colonna P, Nannan N, Guardone A. Multiparameter equations of state for siloxanes: $[(CH_3)_3\text{-Si-}O^{1/2}]_2$-$[O\text{-Si-}(CH_3)_2]_{i=1,3}$, and $[O\text{-Si-}(CH_3)_2]_6$. Fluid Phase Equil 2008;263:115–30.

[17] Barth T, Jesperson D. The design and application of upwind schemes on unstructured meshes. 1989. AIAA Paper 89-0366.

[18] Persico G, Mora A, Gaetani P, Savini M. Unsteady aerodynamics of a low aspect ratio turbine stage: modeling issues and flow physics. ASME J Turbomach 2012;134, 061030 (10 pages).

[19] Reeves CR, Rowe JE. Genetic algorithms: principles and perspectives: a guide to GA theory. Norwell, MA, USA: Kluwer Academic Publishers; 2002. ISBN 1402072406.

[20] Persico G. Evolutionary optimization of centrifugal nozzles for organic vapours. J Phys Conf 2017;821(012015):1–11.

[21] Adams B, Bauman L, Bohnhoff W, Dalbey K, Ebeida M, Eddy J, et al. Dakota: a multilevel parallel object-oriented framework for design optimization, parameter estimation, uncertainty quantification, and sensitivity analysis: version 6.6 users manual. 2017. Sandia Technical Report SAND2014-4633.

[22] Denos R, Arts T, Paniagua G, Michelassi V, Martelli F. Investigation of the unsteady aerodynamics in a transonic turbine stage. ASME J Turbomach 2001;123(1):81–9.

[23] Miller R, Moss R, Ainsworth R, Harvery N. Wake, shock, and potential field interactions in a 1.5 stage turbinePart I: vane-rotor and rotor-vane interaction. ASME J Turbomach 2003;125(1):33–9.